

Design and Validation of a Novel Robotic Neck Brace for Cervical Traction

Priya Kulkarni¹, *Student Member, IEEE* and Sunil K. Agrawal^{1,2}, *Member, IEEE*

Abstract—Cervical traction is a common and effective treatment for degenerative disk diseases and pain in the cervical spine. However, the manual and mechanical methods of applying traction to the head-neck are limited due to variability in the applied forces and orientation of the head-neck relative to the shoulders during the procedure. Current robotic neck braces are not designed to provide independent rotation angles and independent vertical translation, or traction, to the brace end-effector connected to the head, making them unsuitable for traction application. This work proposes a novel architecture of a robotic neck brace, which can provide vertical traction to the head while keeping the head in a prescribed orientation, with flexion and lateral bending angles. In this paper, the kinematics of the end-effector attached to the head relative to a coordinate frame on the shoulders are described as well as the velocity kinematics and force control. The paper also describes benchtop experiments designed to validate the position control and the ability of the brace to provide a vertical traction force. It was shown that the maximum achievable end-effector orientations are 16° in flexion, 13.9° in extension, and $\pm 6.5^\circ$ in lateral bending. The kinematic model of the active brace was validated using an independent motion capture system with a maximum root mean square error of 2.41° . In three different orientations of the end-effector, neutral, flexed, and laterally bent, the brace was able to provide a consistent upward traction force during intermittent force application. In these configurations, the force error has standard deviations of 0.55, 0.29, and 0.07N, respectively. This work validates the mechanism's ability to achieve a range of head orientations and provide consistent upward traction force in these orientations, making it a promising intervention tool in cases of cervical disk degeneration.

Index Terms—Parallel Mechanisms, Kinematic Analysis, Rehabilitation Robots

I. INTRODUCTION

Cervical spondylosis is a disease that refers to age-related degeneration of the cervical spine [1]. This disk degeneration affects approximately 80-90% of people over the age of 50 [2]. Spondylosis can cascade into a variety of subsequent neck deformities, including cervical radiculopathy, which is a disorder caused by nerve root dysfunction [3] [1]. These deformities can cause weakness in the upper or lower extremities and difficulty with fine motor tasks [4]. Furthermore, the pain and dysfunction associated with cervical disk degeneration can negatively affect quality of life and interfere with the ability to complete activities of daily living [5].

¹P. Kulkarni and S. K. Agrawal are with the Robotics and Rehabilitation Laboratory, Department of Mechanical Engineering, Columbia University, New York, NY 10027 USA (e-mail: pk2689@columbia.edu).

²S. K. Agrawal is with the Department of Rehabilitation and Regenerative Medicine, Columbia University Medical Center, New York, NY 10032 USA (e-mail: sunil.agrawal@columbia.edu).

While surgery can correct some degenerative disk conditions [6], it increases the risk of complications [7]. In order to mitigate the risks associated with surgery, non-operative methods are used to treat cervical disk disease. A survey concluded that 93.1% of physical therapists use traction as a method for treating nerve root compression caused by cervical radiculopathy [8]. In a clinical setting, manual and mechanical traction methods are used to treat patients [8].

During manual traction, the patient's head and neck are manipulated by a trained physical therapist or a physician. The head is moved in a variety of orientations, and traction is applied as the clinician sees fit [9]. Manual traction provides the clinician with the most freedom to manipulate the position and orientation of the head, but suffers from the error intrinsic to human manipulation. When clinicians deliver traction forces manually within coarse categories of 0-20N, 20-50N, and 50N+, they are able to achieve the correct level only 75% of the time [10].

Mechanical traction is a common method of applying cervical traction, where the patient lies in a supine position with the head flexed forward on a cradle [11]. As nomenclature, flexion and extension are rotational movements in the sagittal plane, where the chin is moving towards or away from the chest, respectively. This cradle is attached to a machine that moves on a track in a direction away from the shoulders parallel to the cervical spine. Mechanical traction has an advantage over manual traction as it has more precise control over both the head position and the magnitude of forces applied during traction. It can also provide intermittent traction to the patient during which the traction force cycles between high and low values with specific timing. Intermittent traction has been shown to decrease pain in people with cervical radiculopathy and reduce the effect that the disease has on their activities of daily living [12]. Intermittent traction has also been shown to outperform continuous traction in reducing pain and increasing mobility [13].

Another form of mechanical traction is over-the-door traction for at-home use [14]. In this method, the user wears a head halter, which is fitted around the base of the head under the skull [15]. The halter is connected to a water bag on a pulley, which provides an upward force on the head. In patient groups with cervical radiculopathy, over-door traction was found to lower neck disability and pain [16]. Both forms of mechanical traction have limited control over the angle of the head, and neither allows for rotation in the frontal plane, also known as lateral bending. The ability to provide traction force in a lateral bending position has been shown to improve cervical range of motion and reduce neck pain

[17]. Therefore, it is important to include this capability in a traction device, but there is no mechanical traction method that can keep the head in a laterally bent position.

A clear gap exists in this area due to (i) lack of control of the angular orientation of the head during traction and (ii) control of the traction force. Robotic neck braces have recently emerged as a method of prescribing an orientation of the head or for applying forces. These devices use active linkages between the shoulders and the head to control head movement, making them attractive options for the application of cervical traction. However, existing robotic neck brace architectures have limitations in the application of cervical traction. Robotic neck braces that are focused on head rotation lack the ability to provide an independent vertical translation to the head [18]. Similarly, other proposed cable-driven dynamic neck brace designs have 3 rotational degrees-of-freedom, but lack independent vertical translation [19]. While a 6 degree-of-freedom mechanism has been designed, using the architecture of a Stewart platform, it was not aimed at exploring traction force application [20]. Another mechanical traction device was designed and tested for the application of cervical traction in a surgical setting [21]. This device can provide a traction force, with a manually prescribed flexion angle, but does not provide control over the lateral bending angle.

Two neck devices were proposed for traction application that use a 3RPS structure as the architecture of the brace [22] [23]. However, the motion of these mechanisms is not ideal for traction. This is due to the coupling of the axial rotation angle to the lateral bending and flexion-extension angles of the end-effector. *During traction, therefore, the clinician would not be able to command an angle of lateral bending or flexion without also affecting the axial rotation of the head-neck.* Therefore, a different architecture must be chosen to decouple the axial rotation motion from the other two rotations while also allowing independent vertical translation. These gaps in the current literature motivate the work presented in this paper.

A. Motivation and Novelty

Existing methods of applying traction have limitations either due to human variability or physical inability to provide traction to a patient in a lateral bending orientation. Robotic neck braces, while allowing both flexion-extension and lateral bending, currently cannot independently control the vertical translation.

Therefore, a novel architecture of a robotic neck brace is proposed with three chains, which can independently control vertical translation, each consisting of an RPUR structure. This architecture of the parallel mechanism was included in a collection of possible parallel mechanisms in [24]. However, detailed analysis and design of mechanisms with this architecture have not been reported in the literature or pursued for this application. Due to the specific architecture of the individual chains of the parallel robot, it can be verified, using the principles of screw theory, that the end-effector has an independent vertical translation in the inertial

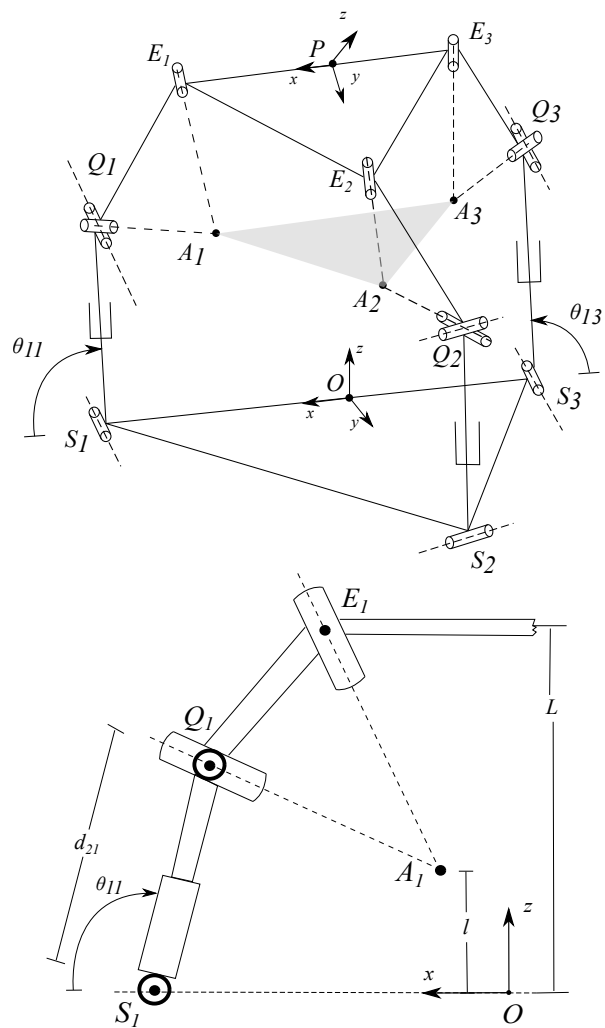


Fig. 1. (Top) Schematic of overall Brace: The base frame is defined by the shoulders, with an origin at point O . The end-effector frame is at the head and has an origin at point P . (Bottom) A schematic of chain 1 of the mechanism.

frame aligned with the shoulders. This work proposes the first traction device that can apply an independent vertical translation to the end-effector, along with degrees-of-freedom of the end-effector in both flexion-extension and lateral bending. The brace was designed, constructed, and validated to demonstrate these features in this paper.

II. MATHEMATICAL MODEL

A. Mechanism Architecture

The brace has three RPUR chains, and the end-effector has three degrees-of-freedom. This structure provides flexion, extension, lateral bending, and vertical translation roughly parallel to the cervical spine relative to the shoulders. A three-chain mechanism was selected to be placed around the head and shoulders in a wearable application. Each chain has the same RPUR structure. The chains are placed such that the axes of the first revolute joints (S_i) for chains 1 and 3 are parallel to each other and perpendicular to the axis of the first revolute joint of chain 2 (See Fig.1). The universal

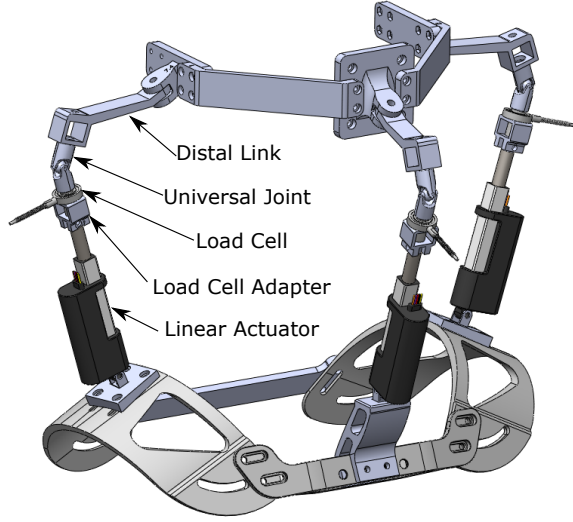


Fig. 2. Brace CAD with chain 1 parts labeled.

joint consists of two revolute joints, whose axes intersect at the point Q_i . The axis of the second revolute joint on the universal joint and the axis of the final revolute joint on the chain intersect at the points A_i . The prismatic joints between S_i and Q_i are the active joints in this design.

A CAD model of the device is displayed in Fig. 2 where chains 1 and 3 sit on the left and right shoulders, respectively, while chain 2 is attached behind the neck, taking support from the shoulders. The end-effector of the device is designed as a headband around the forehead of the wearer.

Examination of the constraints on key points of the mechanism reveals that A_1 and A_3 are constrained to the xz plane of the base frame. Therefore, the plane created by A_i cannot rotate about the z -axis. Since the plane A_i is on the rigid body of the end-effector, it can be concluded that the end-effector cannot rotate about the z -axis and the rotation in the horizontal plane (α) must be zero.

B. Inverse Kinematics

The prismatic joint lengths in chains 1, 2, and 3 (d_{21}, d_{22}, d_{23}) were computed given a desired end-effector flexion angle (β), lateral bending angle (γ), and vertical position (${}^{F_O}P_z$). The rotation matrix ${}^O R_P$ of the base frame, F_O , to the end effector frame, F_P , was described as a Space 3-1-2 rotation with angles $[\alpha, \beta, \gamma]$.

$${}^O R_P = \begin{bmatrix} s\alpha s\beta s\gamma + c\gamma & s\beta s\gamma - c\gamma s\alpha & c\beta s\gamma \\ s\alpha c\beta & c\alpha c\beta & -s\beta \\ s\alpha s\beta c\gamma - s\gamma & c\alpha s\beta c\gamma + s\gamma s\alpha & c\beta c\gamma \end{bmatrix}$$

where s and c are abbreviations for \sin and \cos , respectively.

As previously established, $\alpha = 0$, which allows the rotation matrix to be simplified further.

$${}^O R_P = \begin{bmatrix} c\gamma & s\beta s\gamma & c\beta s\gamma \\ 0 & c\beta & -s\beta \\ -s\gamma & s\beta c\gamma & c\beta c\gamma \end{bmatrix}$$

The locations of A_i and E_i in the base frame were computed using the rotation matrix from the base frame to the end-effector frame, ${}^O R_P$, where i refers to the chain being analyzed.

$${}^{F_O}A_i = {}^{F_O}P + {}^O R_P {}^{F_P}A_i, i = 1, 2, 3 \quad (1)$$

$${}^{F_O}E_i = {}^{F_O}P + {}^O R_P {}^{F_P}E_i, i = 1, 2, 3 \quad (2)$$

Due to the constraints on the y positions of A_1 and A_3 , as well as the constraint on the x position of A_2 , a relationship was computed between the angles β , γ , and the Cartesian positions of the end-effector. By setting the expressions for A_{1y} and A_{2x} equal to zero, the relationship between these values was found and is displayed in (3). For simplicity, the position of the origin on the end-effector in the base frame will be written as x , y , and z , moving forward in the paper.

$$\begin{aligned} y &= -{}^{F_P}A_{1x}c\beta - s\beta(L-l) \\ x &= -{}^{F_P}A_{2y}s\beta s\gamma + c\beta s\beta(L-l) \end{aligned} \quad (3)$$

The lengths $\|E_i Q_i\|$ and $\|A_i Q_i\|$ are constants and known. Using these lengths, two equations were created for each chain i .

$$\|{}^{F_O}A_i - {}^{F_O}Q_i\|^2 = \|A_i Q_i\|^2 \quad (4)$$

$$\|{}^{F_O}E_i - {}^{F_O}Q_i\|^2 = \|E_i Q_i\|^2 \quad (5)$$

$$i = 1, 2, 3$$

Equations (4) and (5) are simplified and recombined into (6) and (7). The values of a_{1i} , a_{2i} , a_{3i} , a_{4i} , a_{5i} , and a_{6i} are known given the end-effector orientations $[\beta, \gamma, z]$.

$$(a_{1i} - b_{1i})^2 + (a_{2i} - b_{2i})^2 = a_{3i} \quad (6)$$

$$(a_{4i} - b_{1i})^2 + (a_{5i} - b_{2i})^2 = a_{6i} \quad (7)$$

where,

$$b_{1i} = d_{2i} \sin \theta_{1i}$$

$$b_{2i} = d_{2i} \cos \theta_{1i}$$

Using the trigonometric identity $s^2\theta_{1i} + c^2\theta_{1i} = 1$, (6) and (7) were simplified and combined to create a matrix equation, where a_{7i} and a_{8i} are functions of a_{1i} , a_{2i} , a_{3i} , a_{4i} , a_{5i} , a_{6i} , and d_{2i} .

$$\begin{bmatrix} a_{1i} & a_{2i} \\ a_{4i} & a_{5i} \end{bmatrix} \begin{bmatrix} s\theta_{1i} \\ c\theta_{1i} \end{bmatrix} = \begin{bmatrix} a_{7i} \\ a_{8i} \end{bmatrix} \quad (8)$$

After solving for $s\theta_{1i}$ and $c\theta_{1i}$, the trigonometric identity $s^2\theta_{1i} + c^2\theta_{1i} = 1$ was used again to yield the following scalar equation.

$$\begin{aligned} (a_{5i}a_{7i} - a_{2i}a_{8i})^2 + (-a_{4i}a_{7i} + a_{1i}a_{8i})^2 \\ = (a_{1i}a_{5i} - a_{2i}a_{4i})^2 \end{aligned} \quad (9)$$

Equation (9) can be solved numerically for each chain to determine the joint lengths $[d_{21}, d_{22}, d_{23}]$ for a commanded β , γ , and z .

C. Forward Kinematics

The forward kinematics of this system is defined as finding the flexion angle, β , the lateral bending angle γ , and the z position of the end-effector, z , given the prismatic joint lengths in chains 1, 2, and 3, i.e. d_{21}, d_{22}, d_{23} . This is accomplished by finding (9) for each chain. This set of three equations relates the three unknown variables, $[\beta, \gamma, z]$, to the known variables d_{21}, d_{22}, d_{23} . All other variables in the equations are known based on the geometry of the brace.

This system of equations can be solved numerically. In order to reduce error due to multiple solutions, an initial guess for the values of $[\beta, \gamma, z]$ is selected. During real-time computation, the initial guess is set as the $[\beta, \gamma, z]$ values of the brace from the previous time step.

D. Jacobian

During force control, the forces of interest are the three Cartesian forces. F_x, F_y , and F_z . Therefore, (6) and (7) were modified such that they were in terms of $d_{2i}, \theta_{1i}, x, y$, and z . The relationships between β, γ, x , and y were previously derived in (3). These equations were then differentiated with respect to time, yielding the following three sets of two equations.

$$A_{1i}\dot{d}_{2i} + B_{1i}\dot{\theta}_{1i} + C_{1i}\dot{x} + D_{1i}\dot{y} + E_{1i}\dot{z} = 0 \quad (10)$$

$$A_{2i}\dot{d}_{2i} + B_{2i}\dot{\theta}_{1i} + C_{2i}\dot{x} + D_{2i}\dot{y} + E_{2i}\dot{z} = 0 \quad (11)$$

$$i = 1, 2, 3$$

where the coefficients $A_{1i}, A_{2i}, B_{1i}, B_{2i}, C_{1i}, C_{2i}, D_{1i}, D_{2i}, E_{1i}, E_{2i}$ are dependent on the brace configuration.

Equation (10) was solved for $\dot{\theta}_{1i}$ and substituted into (11). This results in 3 equations which can be combined to create the matrix equation (12) which relates the joint velocities to the Cartesian end-effector velocities.

$$H \begin{bmatrix} \dot{d}_{21} \\ \dot{d}_{22} \\ \dot{d}_{23} \end{bmatrix} = K \begin{bmatrix} \dot{x} \\ \dot{y} \\ \dot{z} \end{bmatrix} \quad (12)$$

where

$$H = \begin{bmatrix} A_{21} - \frac{A_{11}B_{21}}{B_{11}} & 0 & 0 \\ 0 & A_{22} - \frac{A_{12}B_{22}}{B_{12}} & 0 \\ 0 & 0 & A_{23} - \frac{A_{13}B_{23}}{B_{13}} \end{bmatrix}$$

$$K = \begin{bmatrix} C_{21} - \frac{B_{21}C_{11}}{B_{11}} & D_{21} - \frac{B_{21}D_{11}}{B_{11}} & E_{21} - \frac{B_{21}E_{11}}{B_{11}} \\ C_{22} - \frac{B_{22}C_{12}}{B_{12}} & D_{22} - \frac{B_{22}D_{12}}{B_{12}} & E_{22} - \frac{B_{22}E_{12}}{B_{12}} \\ C_{23} - \frac{B_{23}C_{13}}{B_{13}} & D_{23} - \frac{B_{23}D_{13}}{B_{13}} & E_{23} - \frac{B_{23}E_{13}}{B_{13}} \end{bmatrix}$$

Therefore, the velocity kinematics of the mechanism can be described as follows.

$$\begin{bmatrix} \dot{x} \\ \dot{y} \\ \dot{z} \end{bmatrix} = J \begin{bmatrix} \dot{d}_{21} \\ \dot{d}_{22} \\ \dot{d}_{23} \end{bmatrix} \quad (13)$$

where $J = K^{-1}H$.

Simulation analysis confirms that the matrix K remains invertible throughout the range of motion of the mechanism.

E. Force Control

Due to the constraints on the degrees-of-freedom of the mechanism, there is a relationship between select Cartesian velocities and angular velocities of the end-effector. The relationships between the measure numbers of angular velocity of the end-effector and the rate of change of the Euler angles in a Space 3-1-2 rotation are available in [25]. As $\alpha = 0$, the equations can be further simplified.

$$\begin{aligned} \omega_1 &= \dot{\beta} \\ \omega_2 &= \dot{\gamma}c_\beta \\ \omega_3 &= -\dot{\gamma}s_\beta \end{aligned} \quad (14)$$

where ω_i are the measure numbers of the angular velocity of the end-effector along the coordinate directions of the end-effector.

The time derivative of the position constraint equations in (3) can be computed using a symbolic toolbox, yielding the following equations, where the coefficients f, g, h are dependent on brace geometry and configuration.

$$\begin{aligned} \dot{x} &= f\dot{\beta} + g\dot{\gamma} \\ \dot{y} &= h\dot{\beta} \end{aligned} \quad (15)$$

These equations can be solved for $\dot{\beta}$ and $\dot{\gamma}$, which can then be substituted into (14), resulting in three equations that relate the components of the angular velocity and Cartesian velocity of the end-effector. These equations can then be put into matrix form, yielding the velocity constraint matrix G .

$$\begin{bmatrix} \omega_1 \\ \omega_2 \\ \omega_3 \end{bmatrix} = \underbrace{\begin{bmatrix} 0 & \frac{1}{h} & 0 \\ c_\beta & -\frac{f c_\beta}{gh} & 0 \\ -s_\beta & \frac{f s_\beta}{gh} & 0 \end{bmatrix}}_G \begin{bmatrix} \dot{x} \\ \dot{y} \\ \dot{z} \end{bmatrix} \quad (16)$$

The joint actuator forces $[F_1, F_2, F_3]$ can be related to the end-effector forces and moments by equating the rate of work done by the actuators to the rate of work done on the environment by the end-effector.

$$[F_1 \quad F_2 \quad F_3] \dot{q} = F^T \dot{X} \quad (17)$$

where $F^T = [F_x, F_y, F_z, M_x, M_y, M_z]$, the end-effector forces exerted on the environment, $X = [\dot{x}, \dot{y}, \dot{z}, \omega_1, \omega_2, \omega_3]$, and $\dot{q} = [\dot{d}_{21}, \dot{d}_{22}, \dot{d}_{23}]$.

On substituting (16) into (17) and collecting terms, we get the following force relationship

$$[F_1 \quad F_2 \quad F_3] = ([F_x \quad F_y \quad F_z] + [M_x \quad M_y \quad M_z] G)J \quad (18)$$

It is important to observe the structure of (18). As the third column of G consists of all zeros, the third element of $([F_x \quad F_y \quad F_z] + [M_x \quad M_y \quad M_z] G)$ is F_z , the vertical force along the z direction. This feature allows for independent control of vertical traction force.

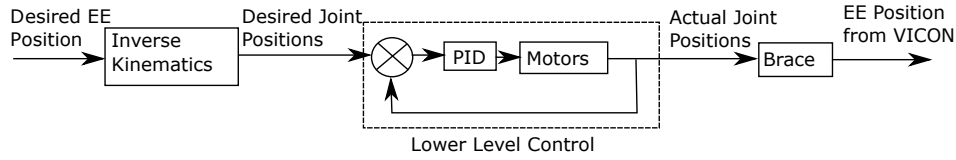


Fig. 3. Position Control Block Diagram, where EE refers to the end-effector

III. METHODS

A. Prototype

The brace is primarily constructed of 3D printed parts, along with off-the-shelf parts for fasteners, joint hardware, motors, and force sensors. The first revolute joint of each chain uses the existing joint axis at the bottom of the linear actuator at S_i , as displayed in Fig. 2. A custom 3D printed adapter was designed to attach one side of a Futek LCM 200 load cell to the end of the linear actuator. Connected to the other side of the load cell is a universal joint, which contains two revolute joints, and is located at the intersection points of the revolute joint axes, at point Q_i . Finally, the distal link is attached to the end of the universal joint and at point E_i , the chain attaches to the headband end-effector.

The Actuonix P16-100-64-12-P linear actuators selected for this mechanism use a DC motor with an integrated encoder to deliver position feedback to the microcontroller. The load cells are connected to Futek amplifiers, which allow the microcontroller to read the forces. This brace utilizes a Photon microcontroller for low-level control of the motors in both position and force control modes. The high-level control is conducted on a desktop computer which streams position or force commands to the microcontroller over WiFi.

B. Position Control

A benchtop experiment was designed to validate position control of the brace. Commands for end-effector orientation and position were sent in a sinusoidal pattern ranging from the minimum to maximum values of flexion-extension movement, lateral bending, and vertical translation. Based on the mathematical model, taking into consideration the stroke length of the linear actuators, the maximum achievable end-effector angles in flexion-extension motion are 21.1° and -16.6° , where the positive and negative values refer to the flexion and extension angles, respectively. The maximum lateral bending angle is 8.25° symmetrically in each direction. In the neutral configuration, the vertical range of motion is 50 mm. The brace was commanded to complete 3 cycles of motion in each direction with a period of 25 seconds.

The linear actuator lengths were computed from the desired position and orientation and were sent to the microcontroller at 50Hz, following the position control block diagram in Fig. 3. A VICON motion capture system was used to measure the achieved position and orientation of the end-effector and the base. Three retroreflective markers were placed near points E_i , and three near points S_i in order to define the end-effector and base frames, respectively. The commanded and achieved joint positions were recorded along

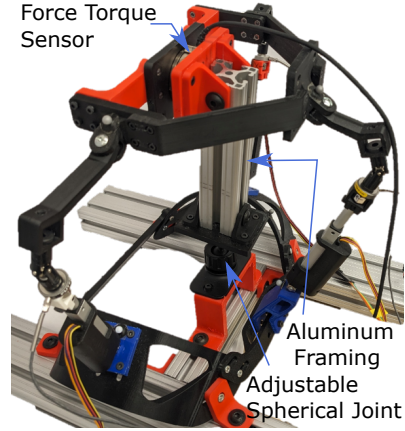


Fig. 4. Force testing apparatus with a six-axis force-torque sensor installed between the brace end-effector and the fixed frame.

with the orientation and position of the end-effector relative to the base frame by using a VICON Lock Lab control box.

C. Force Control

In order to validate the ability of the robotic brace to provide a traction force to the head, the brace was placed in three different configurations, neutral, where flexion and lateral bending angles are set to 0, 10 degrees of flexion, and 5 degrees of lateral bending. These values of flexion and extension were chosen away from the neutral configuration while avoiding the extreme edges of the workspace. The force apparatus displayed in Fig. 4 was designed such that the end-effector of the brace could be configured to a certain position and orientation before being locked into place by the adjustable spherical joint. A piece of aluminum framing was used to fix the end-effector in place. This testbed was designed to imitate human neck movement and validate the device's ability to apply forces in the direction and configurations commonly used during traction. An ATI Mini45 six-axis force torque sensor was connected between the end-effector and the aluminum framing, allowing it to measure the forces exerted by the end-effector on the environment. The origin and axes of the force torque sensor were aligned with those of the end-effector frame.

The control diagram in Fig. 5 depicts the method by which the upward force input was applied to the end-effector, with the lower level control once again occurring on the microcontroller. At each of the previously described positions, a vertical force of 22.3N (5lbs) was commanded for 15 seconds and then the commanded force was set to 0N for 15 seconds, which was repeated 3 times. The remaining end-effector forces and moments were set to be zero. This

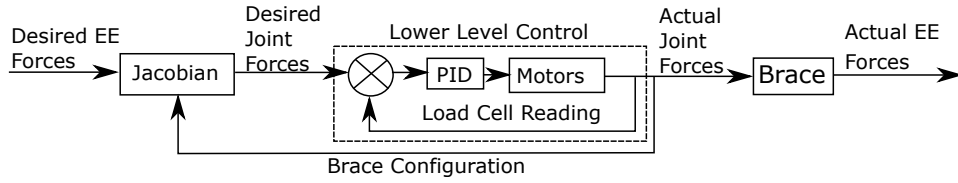


Fig. 5. Force Control Block Diagram

method was chosen to mimic intermittent traction, which generally has a holding time of 10-25 seconds [26]. This force pattern uniquely suits the brace as it requires the timed application and release of traction force.

During vertical force testing, the rise time, steady state error, and maximum out-of-plane forces were collected. Rise time was calculated as the time required for the vertical force to reach its average steady state value from the time the command was sent. The steady-state error was computed as the difference between the commanded force and the average value of the vertical force during the second half of high force application. This timing was selected to allow the mechanism to reach a steady force. The maximum out-of-plane forces were the maximum forces measured in the x and y directions which were commanded to be zero.

IV. RESULTS AND DISCUSSION

The conducted experiments aimed to prove the ability of the robotic traction neck brace to achieve controlled position and orientation control, as well as vertical force control.

A. Position Control

The maximum achieved angles for flexion and extension were 16.01° and -13.9° , respectively. This range of motion includes commonly used flexion angles, which can be around 15° [27] during traction. The maximum lateral bending angles were 6.54° and -6.58° for left and right lateral bending, respectively. The flexion and extension angles achieved by our mechanism is larger than the range of motion of the device proposed in [23], which had maximum flexion and extension angles of approximately 8° . The maximum lateral bending angle is comparable in the two designs with the maximum lateral bending angles of 7° in each direction. When compared with the range of motion in [22], our device has a higher maximum flexion range of 13.5° . However, the right and left lateral bending angles of 20° and 22.1° were higher than those achieved in our device. The mechanism proposed in this paper outperforms both of these mechanisms in flexion. The device in [18] has a higher range of motion in both flexion and lateral bending, 45° and 35° , respectively. Our brace's ability to achieve flexed, laterally bent, and neutral positions demonstrates the device's ability to access different head orientations to apply traction forces. Despite the lateral bending angle being limited relative to other robotic devices, the independently controlled lateral bending and vertical translation of this device are key features that do not exist in current mechanical traction devices.

The ability of the motors to reach commanded positions was measured through the root mean square error (RMSE)

TABLE I
ERROR BETWEEN COMMANDED (C), MEASURED (M), AND EXPECTED (E) POSITIONS

Trial	RMSE C vs E	RMSE E vs M
Flexion Extension	4.72°	2.41°
Lateral Bending	1.97°	1.04°
Vertical Translation	6.03mm	1.56mm

between the commanded and expected end-effector position and orientation based on the motor encoders and the forward kinematics model. The RMSE, as displayed in Table I, remained below 5 degrees in both flexion-extension and lateral bending motion. Fig. 6 displays the two signals through the duration of each position trial. A major source of this error was the delay between when the command was sent to the microcontroller and when the motors achieved this position. This delay, likely caused by high gearing ratios, is not expected to negatively impact traction application, as the application happens gradually. The validity of the positional kinematic model can be evaluated by comparing the expected position and orientation of the end-effector to the achieved position and orientation, which is shown in Fig 7. The forward kinematics method described in Section II was used to calculate the expected end-effector orientation based on the recorded motor positions from the integrated encoders. The RMSE was selected as the main error measure between the commanded and measured positions. The maximum RMSE of 2.41° is lower than another robotic neck brace which has a maximum RMSE of 4.9° between the angle measures and motion capture measurements [18].

B. Force Control

The vertical force tests were comprised of a commanded upward traction force in a square wave. Therefore, the average rise times and steady-state errors, along with their respective standard deviations were calculated and are presented in Table II. The commanded force that was validated for vertical traction was 22.3N (5lbs), and it was able to achieve a mean force value of 17.17N and 15.98N in both the neutral and lateral bending configurations. In the flexed configuration, the brace was able to reach 20.39N.

The variability of force application during manual traction drives the need for a robotic traction brace design. The low standard deviations in all three configurations tested (0.55N, 0.29N, 0.07N) illustrate that the device can consistently apply a traction force when applied intermittently. In [28], the amount of cervical traction was gradually applied to the maximum level tolerable by the patient. In this case, the

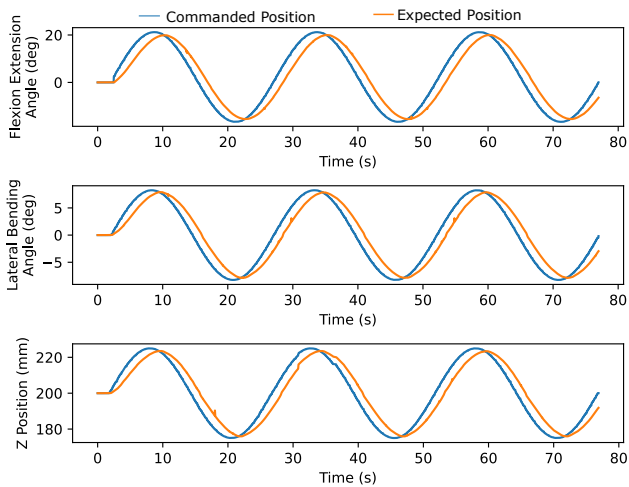


Fig. 6. Command vs. Expected Position from Forward Kinematics

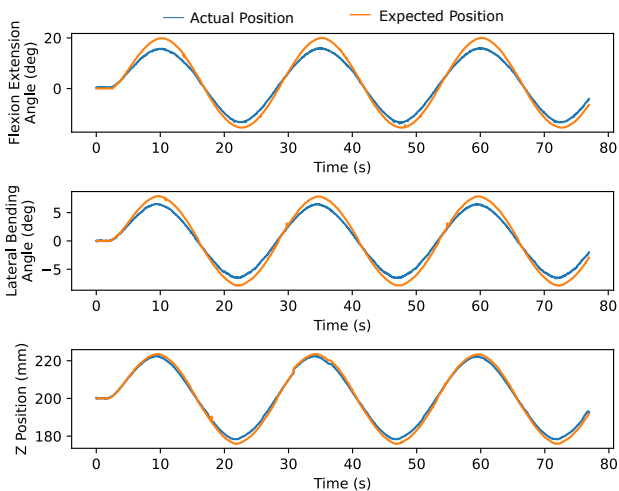


Fig. 7. Expected Position from Forward Kinematics vs. Actual Position

exact force level is not as important as the ability to consistently deliver that same force during traction, especially during intermittent traction. As summarized in Table III, this mechanism combines several abilities in a way not seen in existing traction methods. *The application of vertical force in this experiment demonstrates the first robotic neck brace that can apply vertical force to the end-effector in prescribed degrees of flexion and lateral bending.*

C. Limitations and Future Work

The range of motion in flexion of the brace is smaller than the full range of flexion angles, which may be resolved by changing the alignment of the base frame and the shoulders. In the current design, we have tested traction forces in the range of 20N. While the device proposed encompasses the lower range of forces mentioned in [10] with a high degree of consistency, higher achievable forces would increase its clinical utility. In the future, linear actuators which can provide higher maximum forces will be also considered in the design. We can also increase the traction force magnitude by constructing the linkages out of a less flexible material

TABLE II
VERTICAL FORCE CONTROL ANALYSIS

Configuration	Rise Time (s)	Steady State Error (N)	Max F_x (N)	Max F_y (N)
Neutral	3.11 ± 1.54	5.07 ± 0.55	-2.87	3.82
Flexion	4.48 ± 0.42	1.85 ± 0.29	-3.60	-1.92
Lateral	2.78 ± 0.08	6.26 ± 0.07	1.73	4.18

TABLE III
CAPABILITIES OF TRACTION METHODS AND ROBOTIC NECK BRACES

System	Independent Vertical Translation	Independent Lateral Bending	Controlled Force Magnitude
Manual Traction	Y	Y	N
Mechanical Traction	Y	N	Y
3RRS Device [18]	N	Y	Y
3RPS Device [23] [22]	Y	N	Y
3RPUR Device	Y	Y	Y

such as aluminum. This will reduce the deformation of the linkages and allow higher forces to be applied by the end-effector. While the forces in the x and y directions during traction are low in comparison to the traction force itself, reducing link deformation may further minimize them.

Having validated the brace's ability to provide a controlled traction force, human studies should follow to verify the brace's ability to transmit the force to the human head. Human studies, including observation of muscle activation and comfort of the device, must also be conducted to verify the device's compatibility with human users. Further investigation to explore the brace's potential to apply traction on patients with cervical disk degeneration will be conducted. This may include investigations into intermittent traction during lateral bending and complex traction force profiles.

The brace's architecture has additional desirable features which can be explored. For users with anthropometric dimensions different than an average adult, the placement of the brace on the human shoulders and parameters of the brace can be modified to allow for a shorter neck, narrower shoulders, and smaller head circumference. Additional degrees-of-freedom of the end-effector can also be included based on the placement of the virtual points A_i . Additionally, using the same chain structure, a 4 chain mechanism can allow 2 degrees-of-freedom to the end-effector [29]. The architecture described in this paper can be used and modified not only for traction applications, but also for other applications requiring specific control of head movement.

V. CONCLUSION

This work presented the design of an active robotic neck brace that allows the end-effector to have three degrees-of-freedom consisting of flexion/extension, lateral bending, and vertical translation. The novel 3RPUR mechanism provides independent vertical translation to the end-effector that is infeasible to achieve in other design architectures. This fills the previously unmet need for a traction device that can apply consistent traction forces and independently command the lateral bending angle. The validation of the position and

force control of the end-effector of this brace allows potential future studies to apply traction forces on the human head. This brace would enable clinicians to prescribe precise head orientations during activities of daily life such as sitting or standing. Additional capabilities such as lateral bending and intermittent traction provide an avenue for clinicians to explore new treatment methods. Benefits afforded by this brace could improve clinical treatment and at-home pain relief for many people afflicted with cervical spine diseases.

VI. ACKNOWLEDGEMENTS

We acknowledge research support from the ALS Association (21-MALS-568), Columbia University School of Engineering seed funding through the STAR program, the New York State Spinal Cord Injury Research Board (NYS SCIRB) Institutional Grant (C38336GG), the NYS SCIRB Predoctoral Fellowship (C39062GG), and the National Institutes of Health (1 R21HD110868 - 01A1).

REFERENCES

- [1] N. Theodore, "Degenerative cervical spondylosis," *New England Journal of Medicine*, vol. 383, no. 2, pp. 159–168, July 2020, doi: 10.1056/NEJMra2003558.
- [2] W. Brinjikji, *et al.*, "Systematic literature review of imaging features of spinal degeneration in asymptomatic populations," *American Journal of Neuroradiology*, vol. 36, no. 4, pp. 811–816, Apr. 2015, doi: 10.3174/ajnr.A4173.
- [3] B. I. Woods and A. S. Hilibrand, "Cervical radiculopathy: epidemiology, etiology, diagnosis, and treatment," *Clinical Spine Surgery*, vol. 28, no. 5, pp. E251–E259, June 2015, doi: 10.1097/BSD.0000000000000284.
- [4] D. L. Corey and D. Comeau, "Cervical radiculopathy," *Medical Clinics*, vol. 98, no. 4, pp. 791–799, July 2014, doi: 10.1016/j.mcna.2014.04.001.
- [5] J. T. King Jr, K. A. McGinnis, and M. S. Roberts, "Quality of life assessment with the medical outcomes study short form-36 among patients with cervical spondylotic myelopathy," *Neurosurgery*, vol. 52, no. 1, pp. 113–121, Jan. 2003, doi: 10.1227/0006123-200301000-00014.
- [6] R. C. Huang, F. P. Girardi, A. R. Poynton, and F. P. Cammisa, "Treatment of multilevel cervical spondylotic myeloradiculopathy with posterior decompression and fusion with lateral mass plate fixation and local bone graft," *Clinical Spine Surgery*, vol. 16, no. 2, pp. 123–129, Apr. 2003, doi: 10.1097/00024720-200304000-00002.
- [7] S. G. Memtsoudis, A. Hughes, Y. Ma, Y. L. Chiu, A. A. Sama, and F. P. Girardi, "Increased in-hospital complications after primary posterior versus primary anterior cervical fusion," *Clinical Orthopaedics and Related Research*, vol. 469, no. 3, pp. 649–657, Mar. 2011, doi: 10.1007/s11999-010-1549-4.
- [8] T. J. Madson and J. H. Hollman, "Cervical traction for managing neck pain: a survey of physical therapists in the united states," *Journal of Orthopaedic & Sports Physical Therapy*, vol. 47, no. 3, pp. 200–208, Mar. 2017, doi: 10.2519/jospt.2016.6914.
- [9] N. Peake and A. Harte, "The effectiveness of cervical traction," *Physical Therapy Reviews*, vol. 10, no. 4, pp. 217–229, Dec. 2005, doi: 10.1179/108331905X68547.
- [10] M. R. Gudavalli, *et al.*, "Clinician proficiency in delivering manual treatment for neck pain within specified force ranges," *The Spine Journal*, vol. 15, no. 4, pp. 570–576, Apr. 2015, doi: 10.1016/j.spinee.2014.10.016.
- [11] N. Graham, *et al.*, "Mechanical traction for neck pain with or without radiculopathy," *Cochrane Database of Systematic Reviews*, no. 3, July 2008, doi: 10.1002/14651858.cd006408.pub2.
- [12] P. Moeti and G. Marchetti, "Clinical outcome from mechanical intermittent cervical traction for the treatment of cervical radiculopathy: a case series," *Journal of Orthopaedic & Sports Physical Therapy*, vol. 31, no. 4, pp. 207–213, Apr. 2001, doi: 10.2519/jospt.2001.31.4.207.
- [13] A. K. Mohammed, F. G. Ebtessam, M. M. Abd Elshafy, and M. E. Ibrahim, "Comparative study between continuous and intermittent cervical traction in treatment of chronic mechanical neck pain," *The Medical Journal of Cairo University*, vol. 91, no. 12, pp. 1301–1307, Dec. 2024, doi: 10.21608/mjcu.2024.342719.
- [14] B. Bagheripour, M. Kamyab, F. Azadina, A. Amiri, and M. Akbari, "The efficacy of a home-mechanical traction unit for patients with mild to moderate cervical osteoarthritis: A pilot study," *Medical Journal of the Islamic Republic of Iran*, vol. 30, p. 386, 2016.
- [15] J. H. Wang, A. H. Daniels, M. A. Palumbo, and C. P. Ebersson, "Cervical traction for the treatment of spinal injury and deformity," *JBJS reviews*, vol. 2, no. 5, p. e4, May 2014, doi: 10.2106/jbjs.rvw.m.00108.
- [16] J. M. Fritz, A. Thackeray, G. P. Brennan, and J. D. Childs, "Exercise only, exercise with mechanical traction, or exercise with over-door traction for patients with cervical radiculopathy, with or without consideration of status on a previously described subgrouping rule: a randomized clinical trial," *Journal of Orthopaedic & Sports Physical Therapy*, vol. 44, no. 2, pp. 45–57, Feb. 2014, doi: 10.2519/jospt.2014.5065.
- [17] D. S. Creighton, D. Marsh, M. Gruca, and M. Walter, "The application of a pre-positioned upper cervical traction mobilization to patients with painful active cervical rotation impairment: A case series," *Journal of Back and Musculoskeletal Rehabilitation*, vol. 30, no. 5, pp. 1053–1059, Jan. 2017, doi: 10.3233/bmr-169644.
- [18] H. Zhang and S. K. Agrawal, "Kinematic design of a dynamic brace for measurement of head/neck motion," *IEEE Robotics and Automation Letters*, vol. 2, no. 3, pp. 1428–1435, July 2017, doi: 10.1109/LRA.2017.2671409.
- [19] M. Shoaib, C. Y. Lai, and A. Bab-Hadiashar, "A novel design of cable-driven neck rehabilitation robot (carneck)," in *2019 IEEE/ASME International Conference on Advanced Intelligent Mechatronics (AIM)*. IEEE, July 2019, pp. 819–825, doi: 10.1109/aim.2019.8868660.
- [20] D. Wu, L. Wang, and P. Li, "A 6-dof exoskeleton for head and neck motion assist with parallel manipulator and semg based control," in *2016 International Conference on Control, Decision and Information Technologies (CoDIT)*. IEEE, Apr. 2016, pp. 341–344, doi: 10.1109/codit.2016.7593585.
- [21] B. A. Sherrod, *et al.*, "Motorized robotic closed cervical traction: Biomechanical proof of concept," *Spine*, pp. 10–1097, Aug. 2023, doi: 10.1097/BRS.00000000000004605.
- [22] P. K. Lingampally and A. S. Arockia Doss, "Design, implementation, and experimental study on 3-rps parallel manipulator-based cervical collar therapy device for elderly patients suffering from cervical spine injuries," in *Handbook of Smart Materials, Technologies, and Devices: Applications of Industry 4.0*. Springer, Nov. 2021, pp. 1–23, doi: 10.1007/978-3-030-84205-5_161.
- [23] M. E.-H. Ibrahim, M. T. El-Wakad, M. S. El-Mohandes, S. A. Sami, *et al.*, "Implementation and evaluation of a dynamic neck brace rehabilitation device prototype," *Journal of Healthcare Engineering*, vol. 2022, Oct. 2022, doi: 10.1155/2022/6887839.
- [24] Z. Huang and Q. Li, "Type synthesis of symmetrical lower-mobility parallel mechanisms using the constraint-synthesis method," *The International Journal of Robotics Research*, vol. 22, no. 1, pp. 59–79, Jan. 2003, doi: 10.1177/0278364903022001005.
- [25] T. R. Kane, P. W. Likins, and D. A. Levinson, *Spacecraft Dynamics*. McGraw-Hill Book Co, 1983.
- [26] T. T. Chiu, J. K.-F. Ng, B. Walther-Zhang, R. J. Lin, L. Ortelli, and S. K. Chua, "A randomized controlled trial on the efficacy of intermittent cervical traction for patients with chronic neck pain," *Clinical Rehabilitation*, vol. 25, no. 9, pp. 814–822, Sept. 2011, doi: 10.1177/0269215511399590.
- [27] D. E. Harrison, R. Cailliet, D. D. Harrison, T. J. Janik, and B. Holland, "A new 3-point bending traction method for restoring cervical lordosis and cervical manipulation: a nonrandomized clinical controlled trial," *Archives of Physical Medicine and Rehabilitation*, vol. 83, no. 4, pp. 447–453, Apr. 2002, doi: 10.1053/apmr.2002.30916.
- [28] C.-H. Lee, S. J. Heo, S. H. Park, H. S. Jeong, and S.-Y. Kim, "The functional and morphological changes of the cervical intervertebral disc after applying lordotic curve controlled traction: a double-blind randomized controlled study," *International Journal of Environmental Research and Public Health*, vol. 16, no. 12, p. 2162, June 2019, doi: 10.3390/ijerph16122162.
- [29] J. Zhou, P. Kulkarni, X. Zhao, and S. K. Agrawal, "Design of a traction neck brace with two degrees-of-freedom via a novel architecture of a spatial parallel mechanism," *Robotica*, 2024.